

# Impact of coastal transportation emissions on inland air pollution over Israel: Utilizing numerical simulations, airborne measurements, and synoptic analyses

D. O. Ranmar,<sup>1</sup> V. Matveev,<sup>2</sup> U. Dayan,<sup>3</sup> M. Peleg,<sup>2</sup> J. Kaplan,<sup>3</sup> A. W. Gertler,<sup>4</sup>  
M. Luria,<sup>2</sup> G. Kallos,<sup>5</sup> P. Katsafados,<sup>5</sup> and Y. Mahrer<sup>1</sup>

Received 3 May 2001; revised 30 October 2001; accepted 19 November 2001; published XX Month 2002.

[1] The detection of high ozone levels over large inland areas in Israel during the early, mid and late summer triggered an analysis of air mass back-trajectories. This, in turn, pointed to the transportation system in the metropolitan coastal Tel Aviv region as the possible origin of the ozone's precursors. To link the daily dynamics of rush hour transportation emissions to inland air pollution, in general, and airborne ozone measurements, in particular, an interdisciplinary modeling system was established. The simulations of transportation-to-inland air pollution integrated transportation, emission factor, atmospheric, transport/diffusion, and photochemical models. The modeling results elucidated a spatial and temporal overlap between the ozone precursors and ozone production. The model simulations indicated east to southeasterly dispersion of the pollution cloud. The results agreed well with both spatial and temporal ozone levels as recorded by aircraft over central Israel, as well as with ground-based monitoring station observations. The impact of the Tel Aviv metropolitan area as well as the Gaza Strip, as pivotal coastal transportation sources for inland air pollution in general and ozone formation in particular, is discussed. The synoptic analysis identified the conditions prevailing when elevated air pollution, and especially high ozone levels, exists over central Israel. The analysis showed that this season features a shallow mixed layer and weak zonal flow, which leads to poor ventilation rates and inhibit efficient dispersion of this secondary pollutant. These poor ventilation rates result in the slow transport of ozone precursors, enabling their photochemical transformation under intense solar radiation during their travel from the coast inland. Under these conditions, model results showed that traffic emissions during the morning rush hour from the Tel Aviv metropolitan area contribute about 60% to the observed ozone concentrations. *INDEX TERMS:* 0345

Atmospheric Composition and Structure: Pollution—urban and regional (0305); *KEYWORDS:* air pollution, numerical atmospheric modeling, transportation model, emission factors, photochemical model, ozone, photochemical aged air mass

## 1. Introduction

[2] Elevated ozone levels, above the Israeli ambient standards, were observed at inland rural sites during the early summer months of 1988 to 1991 [Peleg *et al.*, 1994]. Air mass back-trajectory analyses have shown that only air masses passing over the Tel Aviv metropolitan area caused the elevated ozone mixing ratios at rural sites over central

Israel. Furthermore, the high ratio of NO<sub>x</sub>/SO<sub>2</sub> patently indicates that ozone precursors such as nitrogen oxides (NO<sub>x</sub>), carbon monoxide (CO), and volatile organic compounds (VOC) originate mainly from traffic fossil-fuel combustion (NO<sub>x</sub> represents the sum of NO and NO<sub>2</sub>). These pollutants undergo chemical and photochemical transformations in the presence of solar radiation and atmospheric free radicals [Finlayson-Pitts and Pitts, 1997; Seinfeld and Pandis, 1998] to form ozone. The main source for the ozone precursors emitted along the Israeli coastline is transportation [Peleg *et al.*, 1994]. Since the formation of ozone and other secondary pollutants takes on the order of several hours, significant transport and mixing occurs simultaneously with the chemical reactions [Kley, 1997; Seinfeld, 1989]. Thus increasing urban and commercial activity along the highly populated Israeli coastal region, together with expanding transportation activity in the Gaza region, is expected to strongly affect inland air quality and specifically, to cause increasingly elevated ozone levels.

<sup>1</sup>Department of Soil and Water Sciences, Faculty of Agricultural, Food and Environmental Quality Sciences, Hebrew University of Jerusalem, Rehovot, Israel.

<sup>2</sup>Environmental Science Division, School of Applied Sciences and Technology, Hebrew University of Jerusalem, Jerusalem, Israel.

<sup>3</sup>Department of Geography, Hebrew University of Jerusalem, Jerusalem, Israel.

<sup>4</sup>Desert Research Institute, Reno, Nevada, USA.

<sup>5</sup>Laboratory of Meteorology, University of Athens, Athens, Greece.

[3] The effects of vehicular transport emissions have prompted studies in various disciplines, including the following: particulate composition of the atmosphere [Fraser *et al.*, 1999; Staehelin *et al.*, 1998], potential mutagenic activity [Kleindienst *et al.*, 1992], the mode of city air pollution exposure from proximal highways [Roorda-Knappe *et al.*, 1998] and as an integrated component in local-scale air pollution modeling [Pilinis *et al.*, 1993; Moussiopoulos and Papagrorgiou, 1997; Silibello *et al.*, 1998; Svensson, 1998], to name a few. In the latter studies, photochemical grid models were applied to the cities of Athens and Milan to address their regularly recurring air quality problems. These simulations incorporated traffic emissions, together with other metropolitan emitters, as a source of the precursors feeding the simulated atmospheric photochemistry. In these cases, the emission area and the polluted atmosphere overlap spatially, forming what may be viewed as a “self-pollution” phenomenon, where the city is captured as the origin of primary pollutant emissions, and its overlaying atmosphere as the “destination” for their subsequent photochemical transformation products. The involvement of major coastal metropolitan areas in inland ozone pollution was studied in regions such as the San Joaquin Valley in California [Dabdub *et al.*, 1999] and the Los Angeles Basin [Lu and Turco, 1996]. The former study addressed the differential impact of boundary conditions, winds, emissions, and  $\text{NO}_x/\text{VOC}$  sensitivity on the nature of ozone formation, with the San Francisco metropolitan area as one of the model-input pollution sources. It showed that significant inflow into the San Joaquin Valley imposes a strong dependency on the boundary concentration of pollutants and revealed the region as  $\text{NO}_x$ -sensitive, i.e., a dependency of ozone formation on incoming  $\text{NO}_x$  and internally emitted  $\text{NO}_x$  greater than that on VOC influx and emission. The latter work simulated ozone distribution over the Los Angeles Basin, revealing the association of the vertical circulation with sea breeze/mountain winds in the injection process of pollutants into the base of the inversion layer. The elevated reservoir of trapped photochemically aged pollutants may then mix downward to increase surface ozone concentration. Such a mechanism was speculated to take place in Israel, based on the similarities in geography and climate [Dayan and Koch, 1996]. These authors analyzed measurements of the Southern California Air Quality Study (SCAQS) and suggested a possible analogy between the build-up mechanism of inland surface ozone in Israel and the mechanism existing in southern California, due to the similarities between these regions (Mediterranean climate, sea breeze, and terrain features).

[4] The present study addresses the dynamics of transboundary air pollution, where the transportation emissions (such as  $\text{NO}_x$  and VOC) originating from major coastal sources impact the inland mixing layer. The research aimed to resolve the daily influence of rush-hour traffic emissions from these coastal locations on the neighboring inland areas. In this study, we focus on the transportation sources in the Tel Aviv metropolitan and Gaza Strip areas, the main coastal urban areas in the conjugated Israel-Palestinian Authority region. This study includes numerical simulations, their spatial and temporal correlation with airborne-measured ozone from 1994 to 1997, and complementary ground-based measurements performed from June to September of 1999 and 2000.

[5] Since almost no data are available in Israel regarding actual vehicle pollution emission rates, the present study includes measurements performed using the so-called “tunnel technique”. This method gives “real-world” emission rates for the composite vehicle fleet operating on Israeli roads that can be used as input for the transportation model. The data available from aircraft research measurement flights were employed in order to verify the model simulation studies.

## 2. Modeling Systems

[6] Targeting the daily impact of the traffic infrastructure on subsequent spatial and temporal inland air pollution in general and ozone location in particular called for utilizing an integrated interdisciplinary modeling system covering the fields of transportation densities, emission factors, atmospheric dynamics, pollutant transport and diffusion, and photochemistry. For the purpose of this study, the following models were selected: a transportation model (Emme/2, pronounced em-two, named after the French letter “emme” for mobility model) coupled to the emission factor model (EFM), the regional atmospheric modeling system (RAMS) and a transport and diffusion model (TDM). A photochemical module is addressed through a multiple-regression analysis, which found a correlation between ozone mixing ratios,  $\text{NO}_y$  levels and air temperature [Olszyna *et al.*, 1994, 1997] in photochemically aged air masses typical of the region under study [Peleg *et al.*, 1994]. The following subsections address the different modules of the modeling system (2.1–2.5) and provide a brief description of the ground-based measurements (2.6) used in present study.

### 2.1. Transportation Model

[7] The Emme/2 urban/regional transportation system model [INRO Consultants Inc., 1998, and references therein, available at <http://www.inro.ca>] was used to analyze the combination of present transport flow dynamics and land use scenarios, and future conditions regarding transportation system performance. The urban/regional transportation planning and modeling system assesses the balance between travel demand (based on land use) and supply (based on transport facilities) under given scenarios. Land uses are aggregated into analysis zones (such as census tracts), which provide the basis for estimating a matrix of trip origins and destinations. Networks to which the analysis zones are connected represent transport facilities, where each link of the network is characterized in terms of its capacity and speed components. The modeling process produces the desired origin-destination matrices of trips by type of trip, mode of travel and time of day, as well as transport network data which depict the volumes of vehicles and passengers by road segment, travel speed, travel time, and delay time. The traffic flow density (TFD) per hour for each road segment is obtained by multiplying the number of vehicles by the length of the road.

### 2.2. Emission Factor Model

[8] Real world vehicular emission factors for Israel were required to feed the simulation model with the relevant pollution rates. Since almost no data are available for the Israeli scenario, it was necessary to obtain new experimental

measurements. The “tunnel technique” (see experimental section) was employed to enable the calculation of vehicle pollutant emission rate. These rates will represent the accurate makeup (light and heavy-duty mix, percent with catalytic converters, etc) of the vehicles traveling on the Israeli road system.

### 2.3. Atmospheric Modeling

[9] The regional atmospheric modeling system (RAMS) adopted in this study is a state-of-the-art, well-documented mesoscale atmospheric model [Pielke *et al.*, 1992; Walko *et al.*, 1995]. In brief, the RAMS is a multipurpose 3-D versatile numerical prediction model designed to simulate weather systems by calculating multiple meteorological fields (primarily wind, temperature, pressure, and humidity, constructed around the full set of equations in a terrain-following coordinates system, which governs atmospheric motions). The equations are supplemented with optional parameterizations for turbulence, radiation, thermodynamics, clouds, soil type and vegetation. The RAMS is equipped with a multiple grid-nesting scheme that allows a two-way interaction between computational grids of different 3-D resolution. In the current simulation, the RAMS was executed in hierarchical, three-level nested grids to allow zooming in from synoptic scale phenomena through the mesoscale dynamics to the highly resolved local systems. The telescoping from large-scale environment, low-resolution grid cells to small-scale atmospheric systems with fine-meshed, high-resolution grid cells enables small-scale atmospheric features of the target area to be taken into account while simultaneously providing the impact of much larger meteorological systems.

### 2.4. Transport Diffusion Simulation

[10] The transport and diffusion model (TDM) is based on the work of Hurley and Physick [1991], and Physick and Abbs [1991]. It is a Lagrangian 3-D model that simulates the motion of atmospheric pollutants under the influence of atmospheric flow. The TDM was applied to a high-resolution grid with a vertical grid resolution of 50 m and up to a height of 2 km. The TDM was initiated and driven by the meteorological fields produced by the RAMS and interpolated in time and space to the location of the pollutant elements. The coupled Emme/2-emission model provided the TDM with the following transportation data (the anthropogenic driving force): (1) the number of traffic sources, (2) traffic source locations, (3) the emission rates of NO<sub>x</sub> and VOC.

### 2.5. Photochemical Calculation

[11] Quantitative estimation of inland ozone mixing ratios in photochemically aged air masses was established by incorporating a multivariate linear regression analysis [Olszyna *et al.*, 1997] into the TDM model:

$$[O_3] = 9.33 \times [NO_y(\text{ppbv})] + 2.42[\text{Temperature}(^{\circ}\text{C})] - 28.18$$

Here, NO<sub>y</sub> is the sum of all nitrogen oxide species, excluding N<sub>2</sub>O. Results from measurements performed at a rural inland site in Israel [Peleg *et al.*, 1994] have shown that the above equation is also suitable for use in the present study. The application of this equation under the aforementioned conditions enabled the quantification of ozone formation in

our cases. This assumption is based on the fundamental correlation found to exist between NO<sub>y</sub> concentration and the ozone mixing ratio in photochemically aged, NO<sub>x</sub>-limited regimes [Trainer *et al.*, 1993; Olszyna *et al.*, 1994, 1997].

[12] The linear multiple regression model was sequentially operated after each dispersive time step to account for the newly formed ozone. The use of statistical modeling to estimate photochemical production of ozone via association of ozone concentration with meteorological and chemical variables has the advantages of simplicity and a negligible computation time compared to heavy-duty photochemical solvers. Furthermore, the method does not require the differential concentrations of the species participating in the chemical reactions used to initialize and propagate a photochemical model.

## 3. Experimental Design

[13] A detailed description of the research flight, tunnel measurements, and ground level observations is provided in the following subsections.

### 3.1. Research Flights

[14] Research flights were performed over Israel to determine the areas affected by elevated ozone and NO<sub>y</sub> levels and thus to calibrate and test the accuracy of the simulation model. The aircraft used in the investigation was a single-engine Cessna 192. The aircraft was equipped with a high-sensitivity SO<sub>2</sub> analyzer (TEII 43S, pulsed fluorescence method, ±0.1 ppbv sensitivity), a high-sensitivity NO-NO<sub>y</sub> analyzer (TEII 42S, chemiluminescence method, ±0.1 ppbv sensitivity), and an ozone monitor (Dasibi 1008 AH, UV photometric method, ±2 ppbv sensitivity). The zero levels of the monitors were verified both on the ground and in the air, using a PbO scrubber for SO<sub>2</sub>, purafil-activated charcoal for NO<sub>y</sub>, and activated charcoal for ozone. Span calibrations were performed daily on the ground before takeoff. A global positioning system (GPS) was used to continuously monitor the position of the aircraft during the research flight. The data were recorded every 10 s and stored on both a data logger and a personal computer.

[15] All flights were performed during the summer at noon under westerly wind-flow conditions at an altitude of about 300 m (well within the boundary-mixing layer). The flights started at the coast in the Tel Aviv vicinity and attempted to follow the urban pollution plume as it drifted inland, under the westerly wind flows, toward the Judean mountains (up to 1000 m in height). Since photochemical activity is at a maximum at midday and sufficient time has elapsed from peak emission to allow maximum ozone production, the research flights were expected to identify the areas affected by the Tel Aviv pollution plume. Altogether, 32 flights were performed over three different years (1994, 1995, and 1997) in order to cover different periods and hence various meteorological conditions. In the present study, we report the results of three of the research flights, which were used for comparison with the model simulation studies.

### 3.2. Tunnel Experiment

[16] The tunnel technique [De Fre *et al.*, 1994; Pierson *et al.*, 1996] was employed to measure real-world fleet-wide vehicle emission factors for the various pollutants. The

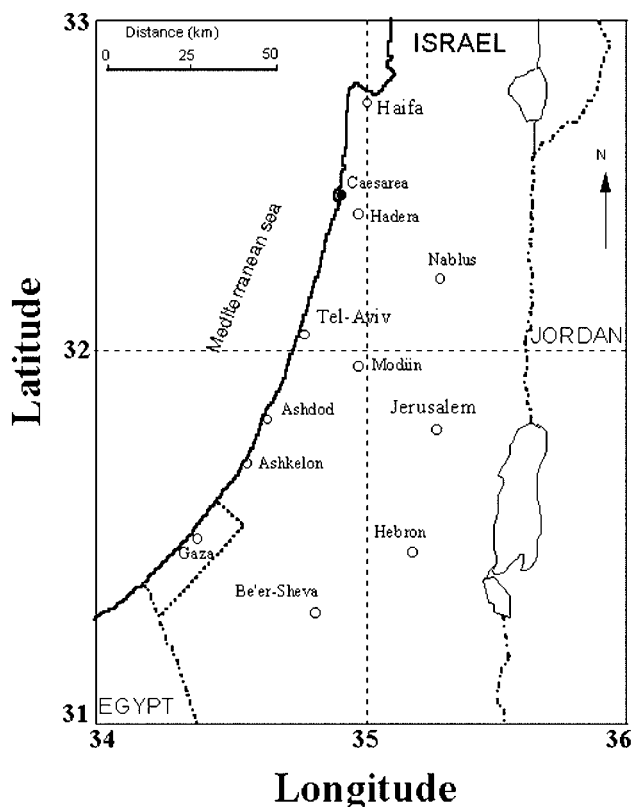


Figure 1. Map of central Israel and the Gaza region.

tunnel, situated south of Jerusalem, is 902 m in length, with an average slope of 3.6% and a cross section of approximately 70 m<sup>2</sup>. Traffic flows in both directions in single lanes. In the tunnel there are 17 sets of blowers to ensure that the CO level remains below 30 ppm at all times. The wind flow in the tunnel is normally in a north-south direction with speeds varying between 1 and 3 m/s. The air sampled for analyses was taken at the northern entrance to the tunnel (background pollution levels) and at a site two-thirds of the way into the tunnel toward the southern exit. Tunnel air was drawn into Tedlar inert sampling bags (30-L capacity) at a rate of about 0.5 L/min. Thus the samples taken for analyses represented hourly averages. The sampled air was immediately analyzed using the following monitors: TEII (Thermo Environment Instruments Inc.) model 42S for NO/NO<sub>x</sub>, TEII 43C for SO<sub>2</sub>, TEII 48 for CO, TEII 41C for CO<sub>2</sub>, Dasibi hydrocarbon analyzer for NMHC (nonmethane hydrocarbons) and a Verewa # F-101 for particulates. Vehicle counts, divided into light- and heavy-duty for each direction, and vehicle speed were taken concurrent to the air sampling. Additionally, wind speed (Met One 010C), temperature and relative humidity (Campbell Scientific Inc. 207) were monitored inside the tunnel. Altogether, 21 hourly samples were taken and analyzed during the research campaign.

**3.3. Ground-Based Measurements and Data Analysis**

[17] Data available from the Israeli national air quality monitoring network provided a variety of chemical and meteorological variables, such as NO<sub>x</sub>, ozone (models 42C and 49C analyzers, respectively, Thermo Environmental Instruments Inc., USA), wind speed and direction, global

sun radiation (GSR) and temperature. The Israeli monitoring network is based on USEPA approved instruments and measuring protocols. The statistical interpretation was based upon data collected between 1 June through 30 September for the years 1999 and 2000. Three locations, the metropolitan area of Tel Aviv, Modiin, and Jerusalem, were chosen, all of which are located within the experimental flight path and along the dominant summertime wind trajectory (see Figure 1).

**4. Model Application**

**4.1. Traffic Flow Simulation**

[18] For the purpose of this study, model implementation focused on detailing existing conditions (reflecting a total population of 6.3 million in the year 2000) to provide input data for a calibration run of the emissions model. The principal steps of the transportation modeling process were the following.

**4.1.1. Trip Generation**

[19] Travel demand (vehicle-trip productions and attractions) was calculated for each of the country's 370 traffic analysis zones based on socioeconomic data for year-2000 conditions (population, housing, vehicle availability, total employment and retail employment). The 1996-97 National Travel Survey for Israel (Central Bureau of Statistics) provides the basis for trip generation rates. Trip attractions were balanced model-wide to total trip productions.

**4.1.2. Trip Distribution**

[20] Matrices of the origin-destination travel patterns were estimated based on the marginal totals from the trip generation step, above, and using a two-way balancing gravity model as calibrated for Israeli conditions (the time-impedance curve can be expressed as the expression impedance = exp(-0.08\*time).

**4.1.3. Travel Assignment**

[21] Matrix origin-destination pairs were assigned to the road network using an incremental capacity-constrained assignment calibrated to Israeli conditions (volume-delay functions adapted from the Department of Transport, Economic Assessment of Road Schemes, United Kingdom, September 1996).

[22] Traffic speeds on road network segments were fed back into the trip distribution model in an iterative process to reflect the effects of traffic congestion on both origin-destination choice and travel-path choice.

**4.2. Vehicle Emission Factors Calculation**

[23] The emission model calculations were based on two complementary methods: the direct and carbon balance method. The direct method essentially produces the EMF of a specific pollutant in the tunnel's air based on the measured pollution concentration, tunnel length, cross section and number of vehicles present during the measurement,

$$EMF_i = (X_i \times V_w \times S \times T) / (L \times N)$$

- EMF<sub>i</sub> emission factor of pollutant i (g/(km × vehicle));
- X<sub>i</sub> pollutant i concentration (g/m<sup>3</sup>);
- V<sub>w</sub> average wind speed in the tunnel (m/s);

**Table 1.** SO<sub>2</sub>, NO<sub>x</sub>, NMHC, and CO Concentration Obtained by the Direct and Carbon Balance Methods<sup>a</sup>

Method	SO <sub>2</sub>	NO <sub>y</sub>	NMHC	CO
Direct	0.38 ± 0.09	4.0 ± 1.0	1.9 ± 0.6	21.0 ± 3.4
Carbon balance	0.34 ± 0.06	3.6 ± 0.6	1.7 ± 0.5	20.1 ± 4.1

<sup>a</sup>Concentration in g/(km per vehicle).

- S cross-sectional area (m<sup>2</sup>);
- T measurement time (s);
- L tunnel length (m);
- N number of vehicles that passed during T.

[24] The carbon balance method EMF is obtained from the following relation:

$$EMF_i = P_i \times C$$

where P<sub>i</sub> is the mass of pollutant i divided by the total carbon in the tunnel air (g/kg C) and C is the average carbon fuel consumption in the tunnel (units of kg C/km).

[25] Calculated emission rates for SO<sub>2</sub>, NO<sub>y</sub>, NMHC and CO are given in Table 1 for average vehicle speeds of 60 to 80 km/h and an average deisel composition of 10%. The results of both methods agree well with one another, indicating the accuracy of the calculated emission values. These emission factors obtained in the present study are compatible with results obtained from similar studies performed both in the United States [Pierson *et al.*, 1966] and Europe [De Fre *et al.*, 1994]. Limited data available from measurements carried out on individual vehicles in Israel also show good agreement with the present study. The results presented in Table 1 were used as input data for the modeling simulation studies since they represent similar conditions (such as speed and vehicle mix) to those expected in the region under examination.

[26] The resulting integrated transportation and emission models provided the emission rate per traffic road segment for each relevant pollutant in units of g/h.

### 4.3. Atmospheric Modeling Aspects

[27] The nonhydrostatic mesoscale-mode, three-way intercalated-nested grid scheme was utilized in the RAMS simulation. The first grid was applied to an area of 1400 × 1400 square km<sup>2</sup> (meso-α scale) [Orlanski, 1975] at a 20-km resolution to derive synoptic phenomena. The latitude and longitude of the northwest and southeast corners of the modeling domain are (32.959, 27.146) and (25.618, 41.681), respectively. The second and third grids were applied to areas of 250 × 350 and 120 × 160 km<sup>2</sup> at 5-km and 1.25 km zooming-in resolutions, respectively. These two more highly resolved grids also account for the sea and land breezes and mountain and valley flows. All simulated zones were centered at the latitude/longitude coordinates of (32.0, 35.0), roughly representing the center of Israel. The simulations were performed for 24 hours starting at midnight. The simulations were initialized and updated every 6 hours with European Center for Medium-Range Weather Forecasts (ECMWF) data fields. The topographic data were obtained from the GTOPO30 project (<http://edcdaac.usgs.gov/gtopo30/gtopo30.html>), which is a global topography digital elevation model (DEM) with a horizontal grid spacing of 30 arc seconds (approximately 1 km) derived from several

raster and vector sources of topographic information. GTOPO30, completed in late 1996, was developed over a three-year period through a collaborative effort led by staff at the U.S. Geological Survey's EROS Data Center (EDC). The dates selected for applying the integrated interdisciplinary modeling system were based on days with high ozone level episodes as recorded by the flight measurements. The ECMWF meteorological fields initialized the simulation at 0000 UTC (0300 LST – local summer time) and provided the boundary conditions for the large-scale grid by updating the calculation at 6-hour intervals to produce the 24-hour atmospheric dynamics simulation. The fields produced by the RAMS were then used to initialize and drive the TDM, dispersing the traffic originated NO<sub>x</sub> and VOC from their emission origins in the Tel Aviv metropolitan area and the Gaza Strip. Applying the statistical multiple regression model following each dispersive time step gave the ozone mixing ratios. However, as mentioned previously, only ozone concentrations obtained in the time domain of photochemically aged air mass were used for inference and analysis, i.e., concentrations obtained about 4 hours (or more) after release.

### 4.4. Rush Hour Determination

[28] Analysis of NO<sub>y</sub> data collected from 1 June to 30 September for the years 1999 and 2000, at a monitoring station located in metropolitan Tel Aviv (see Figure 2), as well as a traffic survey and Emme/2 simulations, indicated that peak traffic emissions occurs between 0600 and 0900 (primarily as NO<sub>x</sub>). This time period corresponds to “rush hour” peak transport loads. From 0900 onward, the NO<sub>y</sub> levels remain monotonically low. This daily time interval therefore reflects the main NO<sub>y</sub> pollution pulse and was used to initialize the simulation runs.

## 5. Results and Discussion

[29] The following section addresses coastal transportation-to-inland trans-boundary air pollution processes as revealed by simulations and airborne/surface-measured ozone levels. Overall three scenarios are analyzed, corresponding to early, mid and late summer ozone episodes as detected by airborne measurements.

### 5.1. Model Simulation

[30] Figure 3 qualitatively illustrates a sequential top view of the NO<sub>y</sub> particles (released from transportation primarily as NO<sub>x</sub>) over the simulation area at 300 m AGL (airborne measurement height for selected hours of the 25 July 1997 ozone episode). The particles were emitted from the Tel Aviv metropolitan and Gaza Strip transportation sources from 0600 to 0900 LST (rush hour). Each particle released represents one gram of pollutant emitted per minute. At 0700 LST, one hour after emission had begun,

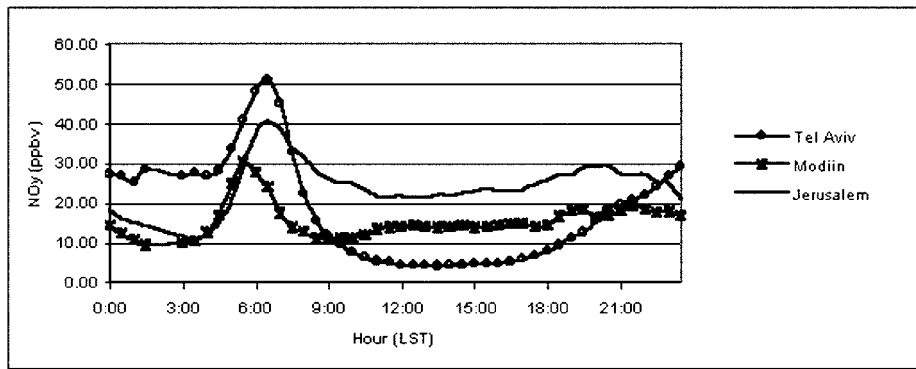


**Figure 2.** Averaged diurnal cycles of measured  $\text{NO}_y$  concentrations in Tel Aviv, Modiin and Jerusalem for the periods of June-September in 1999 and 2000.

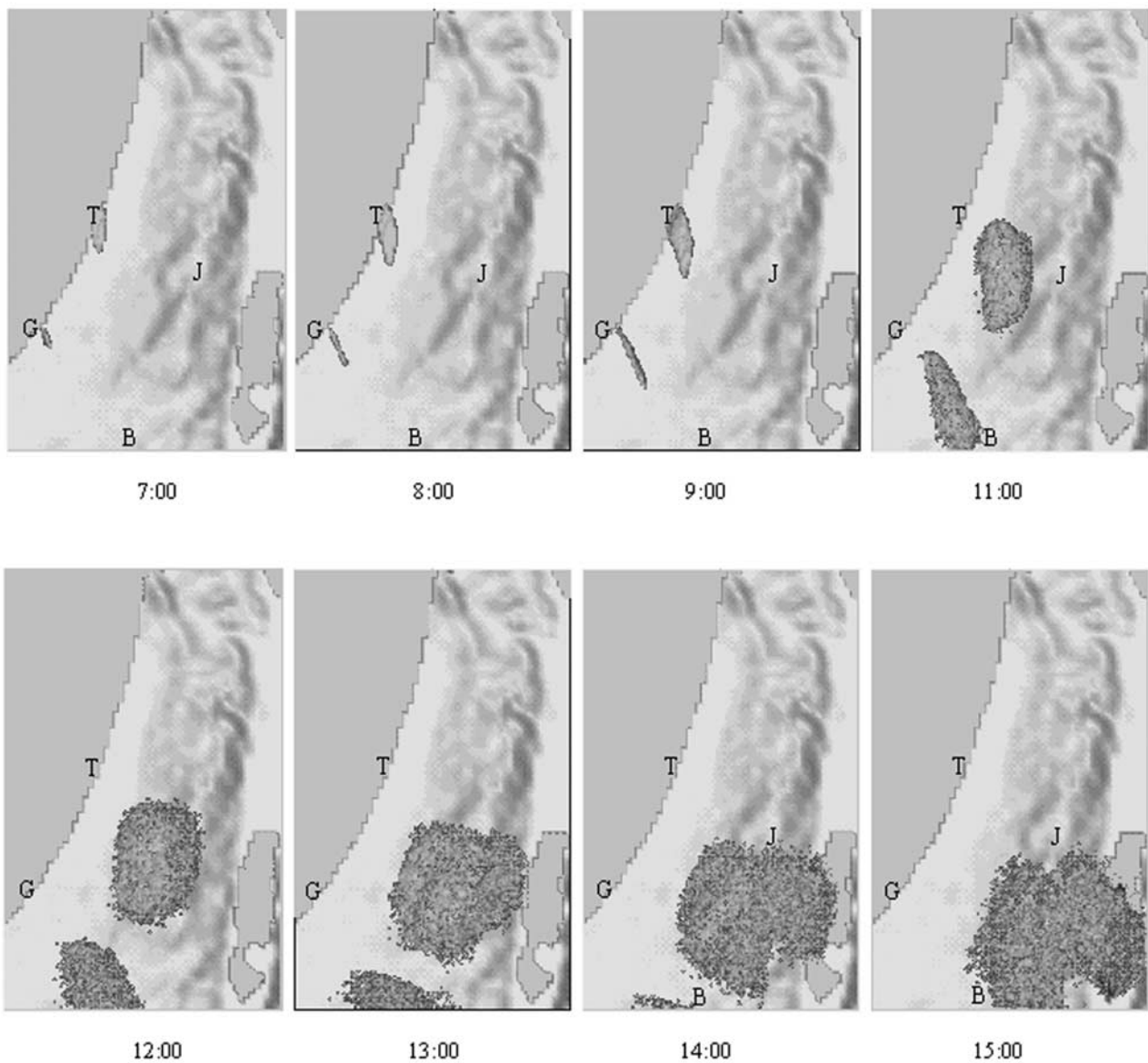


**Figure 3.** Qualitative top view of simulated  $\text{NO}_y$  particles location over Israel at 300 m AGL at selected hours (LST). Particles originated from Tel Aviv metropolitan and the Gaza Strip transportation sources at rush hour, between 0600 and 0900 LST. T, Tel Aviv metropolitan; J, Jerusalem; G, Gaza strip; B, Beer Sheva.

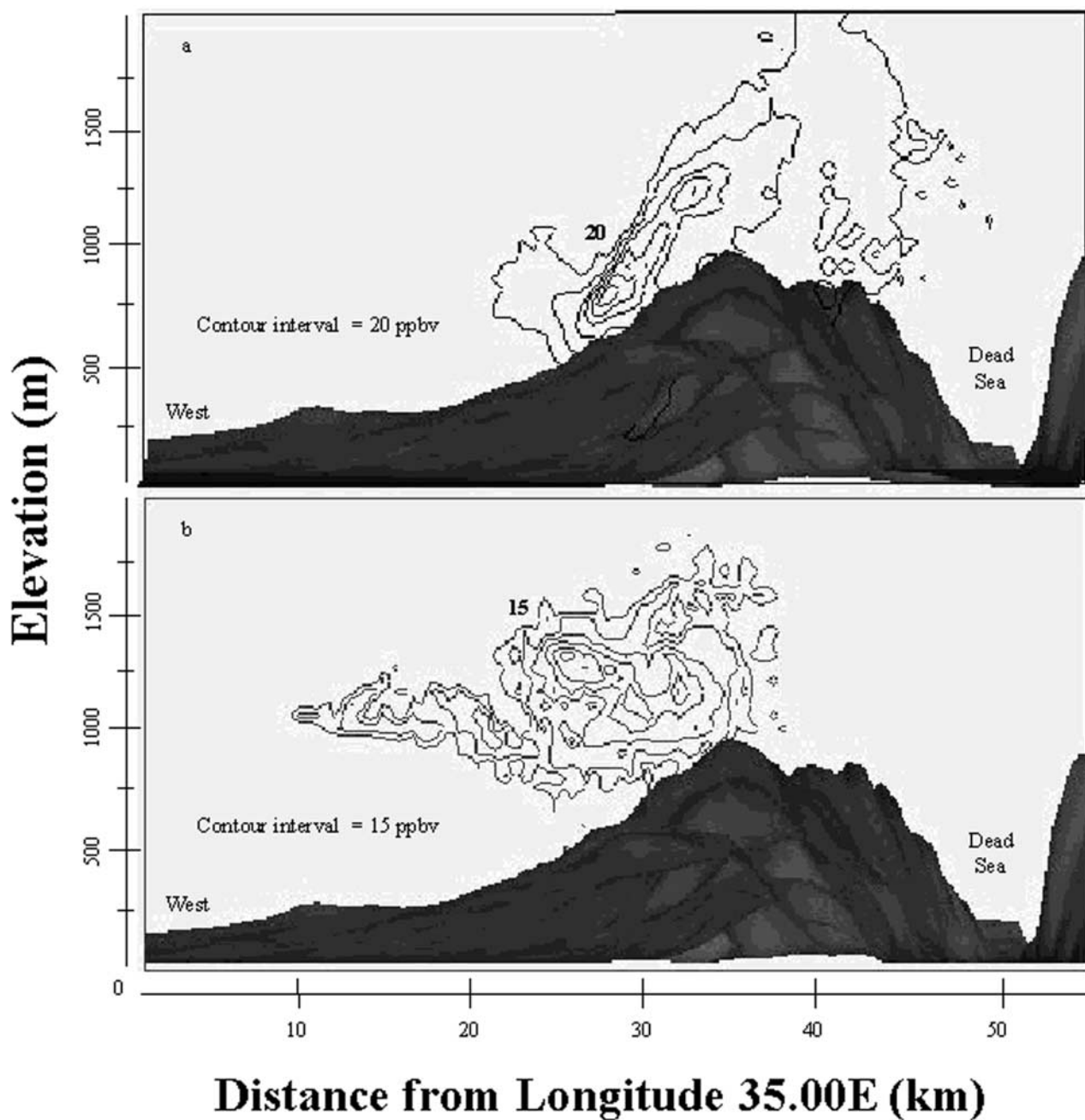


**Figure 4.** Vertical east-west cross section (Y-Z plane) of model-calculated ozone concentrations for (a) 28 August 1997 over Jerusalem area and (b) 25 May 1994 over Beer Sheva area at 1400 LST. Zero distance represents the coast of Tel Aviv. The values of outer contours are indicated. Dark area represents the topography in the studied regions.

particles were transported offshore by an easterly land breeze. During the next 2 hours, with the onset of the Mediterranean sea breeze, the pollution cloud initially located over the sea recirculated inland and mixed with freshly released pollution. Further inland, movement and dispersion of the particles is shown from 1100 to 1500 LST. Two main driving forces manifest the  $\text{NO}_y$  spatial and temporal evolution: east-southeast transport accompanied by a 3-D expansion of the  $\text{NO}_y$  cloud. The particulate clouds from the Tel Aviv metropolis and the Gaza Strip extend to a height of 300 to 400 m (above sea level) by

1100. At 1300, with the inland penetration of the particles over the mountain range coupled with increasing thermal instability, the pollution clouds expand to a height of 1500 m. Almost identical patterns were obtained (not shown) for traffic-produced VOC and CO.

[31] Figure 4 shows a vertical east-west cross section of calculated ozone concentration over Jerusalem (Figure 4a, 28 August 1997) and Beer Sheva (Figure 4b, 25 May 1994) at 1400, viewed from the south. On 28 August 1997, the maximal observed ozone values over Jerusalem ranged from 120 to more than 180 ppbv (Figure 5f), compared to

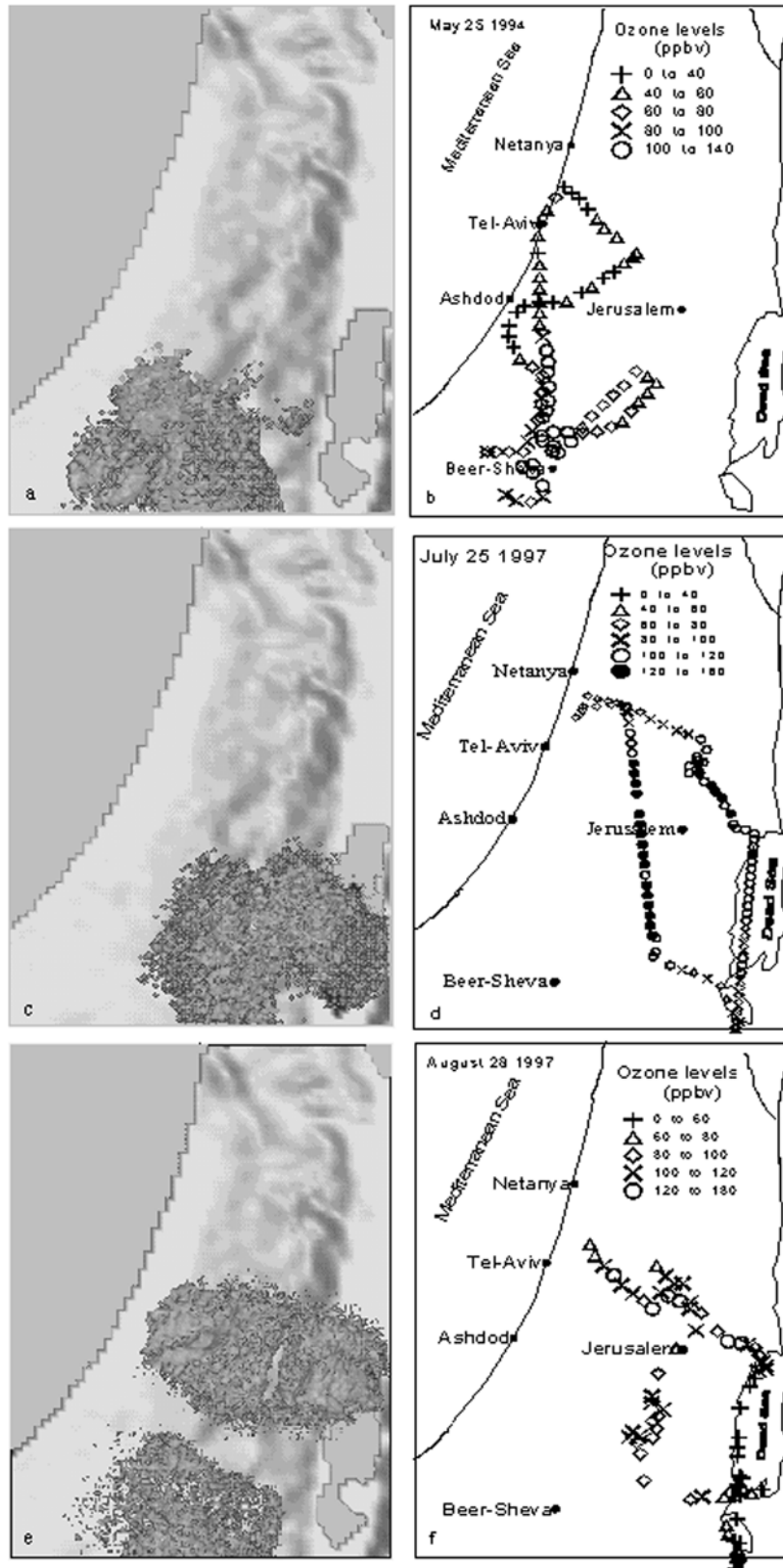


**Figure 5.** Qualitative comparison of model simulation with aircraft measurements of ozone for the three days studied: 25 May 1994, 1400–1600 LST, (a) model simulation and (b) flight measurements; 25 July 1997, 1400–1600 LST, (c) model simulation and (d) flight measurements; 28 August 1997, 1400–1600 LST, (e) model simulation and (f) flight measurements.

calculated values of about 110 ppbv (Figure 4a). On 25 May 1994 (Figure 4b), maximal observed ozone levels over Beer Sheva area ranged from 100 to 160 (Figure 5b). The corresponding calculated maximal values were about 85 ppbv. The explicit inclusion of traffic pollution from metropolitan Tel Aviv during rush hour (0600-0900) suggests that it accounts for more than 60% of the observed inland ozone pollution. The rest may be attributed to (1) background concentrations (up to 60 ppbv in some of the airborne measurements) and (2) alternative ozone sources, such as traffic emissions from other locations.

**5.2. Flight and Model Comparison**

[32] Model results for three scenarios were compared with airborne measurements of ozone concentrations. The inland air pollution episodes represent early (25–26 May, 1994), middle (25 July 1997) and late (28 August 1997) summer. Figure 5 shows the measured ozone levels along the flight path at 1300–1500 LST (Figures 5b, 5d, and 5f) and their corresponding model-calculated photochemically aged O<sub>3</sub> particles (Figures 5a, 5c, and 5e) for 1400. The actual ozone concentrations were presented in Figure 4, while Figure 5 shows their spatial distribution in a qualitative manner.

[33] Analysis of the research flight performed on 25 May 1994 reveals that the simulation study identified the main polluted area over Beer Sheva (Figure 5a). This is in good qualitative agreement with the flight measurements (Figure 5b). The wind field pattern (Figure 6a) traces back to the NNW, essentially originating from the Tel Aviv coastal area. The simulation results for 25 July 1997 (Figure 5c) predict a widely dispersed pollution plume over the central-to-southern Judean Hills with Jerusalem at its northern peak. The research flights for this date (Figure 5d), as well as the calculated wind field (Figure 6b), which exhibits a general west-to-east flow, supports this general pattern. The high concentrations of O<sub>3</sub> measured north of Jerusalem were not captured by the model. This suggests that emission sources from alternative areas (not included in the Tel Aviv morning rush hour traffic emissions) may have contributed to the ozone formation: for example, transportation sources from Jerusalem and noncoastal cities, as well as continuous traffic emissions from the Tel Aviv metropolitan area, besides the rush hour emission (0600–0900). On this day (Figure 6b), the wind field pattern exhibited a northwesterly flow that transported inland pollutants from northern coastal sources (not overlapping the Tel Aviv sources as occurred under a NNW flow, Figures 5a and 5b). Consequently, an extended pollution area north of Jerusalem was measured. The simulation of a late summer episode (28 August 1997) depicted ozone pollution over an extended region of central Israel and over Jerusalem extending to the Dead Sea, and a secondary polluted area to the south over Beer Sheva (Figure 5e). The flight measurements similarly identified the highest ozone levels over central Israel extending to the Dead Sea. It appears that the Jerusalem region was affected by pollution sources originating from the central Israeli coastal plane while the area over Beer Sheva was affected by emissions from the Gaza Strip (Figure 5f). The predicted wind field for the corresponding date (Figure 6c) indicated west-to-south-east flow, resulting in an extended inland air pollution pattern. It's interesting to note that for days dominated by

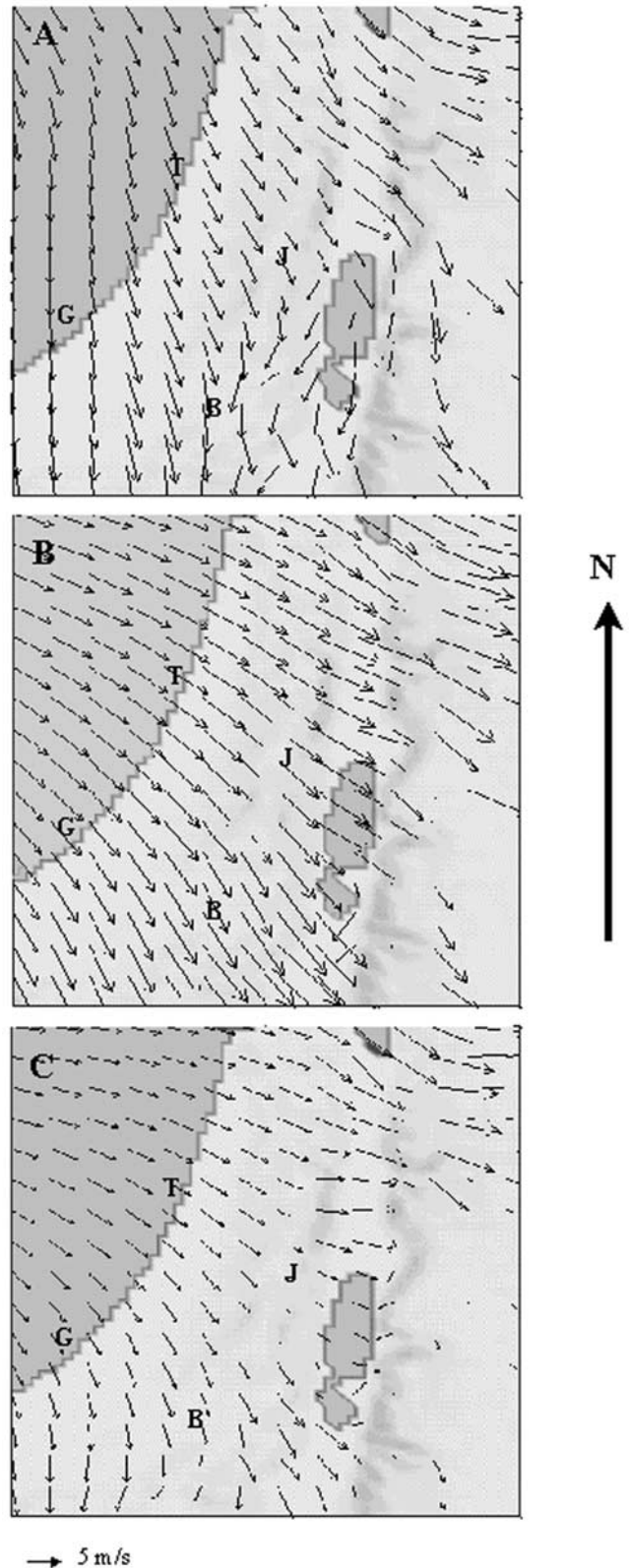


**Figure 6.** Simulated wind fields at Z = 600 m for (a) 25 May 1994, (b) 25 July 1997, and (c) 28 August 1997 at 1200 LST. Wind arrows below topography height are truncated. T, Tel Aviv metropolitan; J, Jerusalem; G, Gaza strip; B, Beer Sheva.

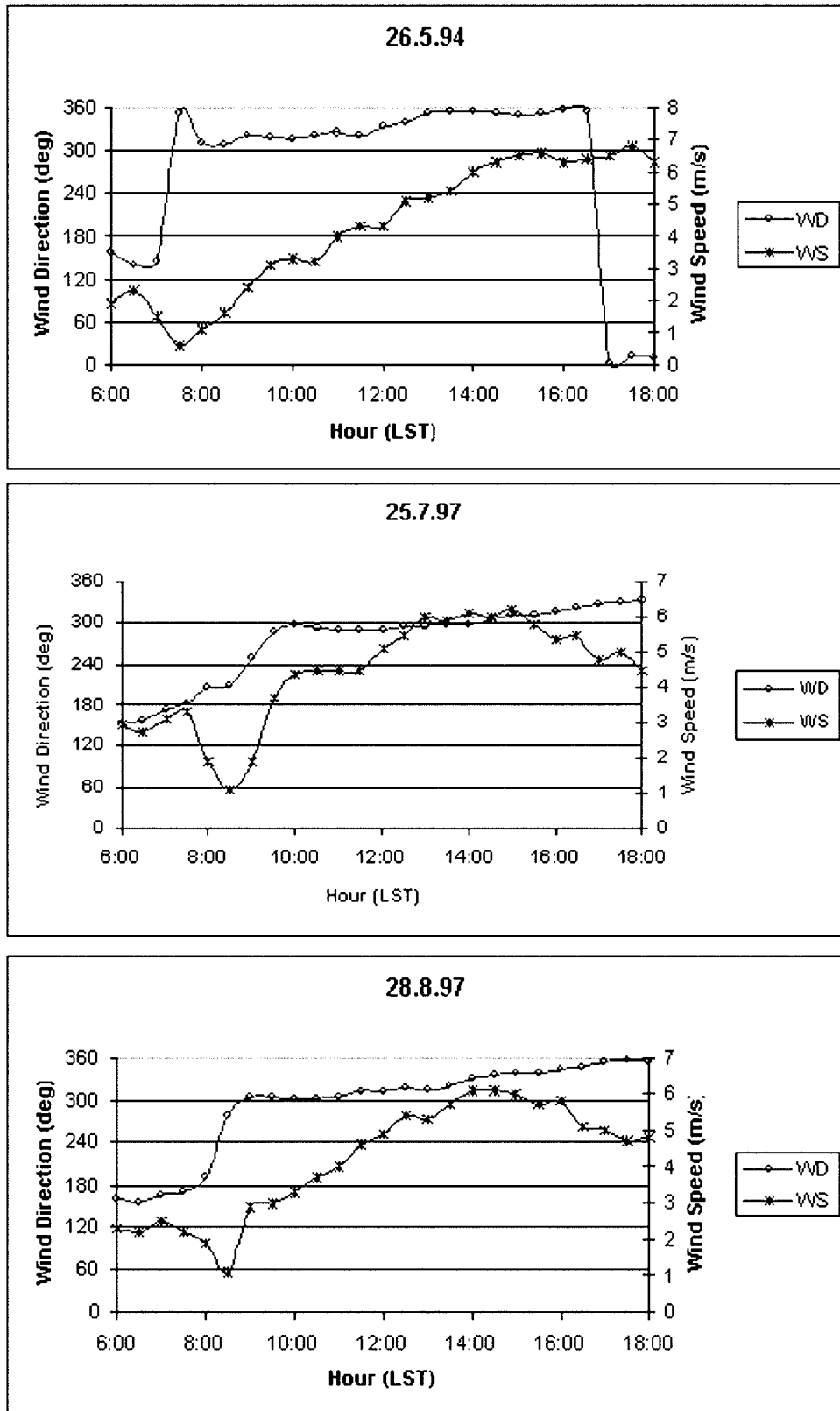


Figure 7. Measured wind direction (WD) and wind speed (WS) in Tel Aviv for 25 May 1994, 25 July 1997, and 28 August 1997 (LST).

**Table 2.** Synoptic and Meteorological Conditions During the Three Elevated Ozone Concentration Episodes Analyzed (Noontime)

Season	Dates	Synoptic Conditions (Surface and Upper Atmospheric Layers)	Resultant Surface Flow	Mixed Layer (ML) Depth	Mean Wind Speed in ML, $m\ s^{-1}$	Ventilation, $m^2\ s^{-1}$	$T_{max\ Jer} - T_{max\ TA}$	$GSR_J - GSR_{TA}^c$ , $Wm^{-2}$
Spring-early summer	25-26 May 1994	Weak warm trough at the surface accompanied by weak zonal flow at 500 hPa atmospheric level	NE inland and NW breeze resulting in a northerly wind along the coast veering to NW inland	350 m capped by a sharp inversion layer	2.5	875	0.7°C	50
Mid-summer	25 July 1997	Weakening of the "Persian Trough" accompanied by a subtropical anticyclone inducing subsidence at mid- and high atmospheric layers	NW sea breeze as the prominent meso-scale system	700 m capped by a subsiding inversion	4	2800	-0.6°C	75
End of summer	28 August 1997	Weakening of the "Persian trough" accompanied by a subtropical anticyclone - inducing subsidence in mid and high atmospheric layers	NW winds caused mainly by the sea breeze veering to W winds farther inland	800 m capped by a subsiding inversion aloft	2.5	2000	0.5°C	110

<sup>a</sup> Ventilation rate; Mixed-layer depth times the mean wind speed in the mixed layer representing the ability of the atmosphere to transport contaminants away from a source region. The average ventilation rate over the Israeli coastal plain for the entire summer ranges from less than  $1000\ m^2\ s^{-1}$  to over  $10000\ m^2\ s^{-1}$ .

<sup>b</sup>  $T_{max\ Jer} - T_{max\ TA}$ : A measure of the intensity of subsidence caused by prominence of the subtropical anticyclone (the upper-air synoptic system that governs the eastern Mediterranean during summer months). A more positive difference indicates more strongly subsiding conditions.

<sup>c</sup>  $GSR_J - GSR_{TA}$ : The difference in maximum global solar radiation between Jerusalem and Tel Aviv. A more positive difference indicates that the inversion behaves like a perfect lid on the atmosphere below it, preventing upward motions and augmenting turbidity aboveground.

southwest winds, low levels of airborne measured ozone (60 ppbv) were detected over central Israel.

[34] Surface wind speed and wind direction measured at a station in Tel Aviv (Figure 7) agrees well with model results (Figures 5a, 5b, and 5c). Both model-predicted and measured data indicate that on 25 May 1994, the early morning NNW winds carried the newly emitted traffic pollution southward (Figure 5a). For the mid-to-late summer episodes (25 July and 28 August 1997), winds veering from west to NW, accompanied by intensified wind speed, dispersed the pollution toward the east and southeast (Figures 5b and 5c).

**5.3. Relation of Air Pollution Scenarios to Weather Conditions**

[35] Spring and early summer are characterized by the overwhelming influence of the subtropical high-pressure system. This situation often leads to a shallow mixed layer accompanied by weak zonal winds. Both of these features result in poor ventilation conditions and consequently to rising air pollution concentrations within the stable profile formed [Dayan and Rodnizki, 1999].

[36] All three episodes of elevated ozone concentration recorded by aircraft measurements and selected for simulation were found to fall into the “shallow Persian trough” synoptic category. This category occurs during warm summer days mainly at the start, but occasionally both in the middle and at the end of the summer season. This synoptic pressure pattern features stagnation conditions that evolve as a result of weak-pressure-gradient winds, a shallow mixed layer capped by subsiding warm and dry air and accordingly poor ventilation within the mixed layer. Several air pollution studies conducted in Israel, mainly over coastal environments, have already identified this synoptic category as being the main one affecting pollutants dispersion [Dayan et al., 1988; Hashmonay et al., 1991; Koch and Dayan, 1992; Dayan and Rodnizki, 1999]. Table 2 describes the main elements influencing the dispersion of pollutants and their measured values for three of the episodes analyzed. The calculated ventilation rates are based on mixing depths measured over the central coastal plain of Israel and are given in order to represent the worst regional transport conditions.

[37] The first case analyzed (25 May 1994) typifies the dispersion conditions associated with the “Weak Persian Trough” mode (Figure 8a). During the noon hour of this episode, a northerly wind blew along the coast up to a few hundred meters above ground within the shallow mixed layer. Both the simulation (Figure 5a) and flight observation (Figure 5b) results indicate transport of the emitted plume southward with very limited dilution. The second episode analyzed (25 July 1997) was characterized by a somewhat deeper “Persian trough” (Figure 8b). The dispersion conditions during this event were much better since the mixed layer was deeper and the resultant onshore winds stronger, leading to three times the ventilation rate measured in the first case. Both the simulation and measurement results (Figures 5c and 5d) show the elongated propagation of the plume during its transport southeast toward the inland elevated region. The “Persian trough” during the third case studied (28 August 1997) is in its weakest mode, leading to weak and variable winds onshore (Figure 8c). Under such dispersion conditions, the polluted air mass drifts very slowly

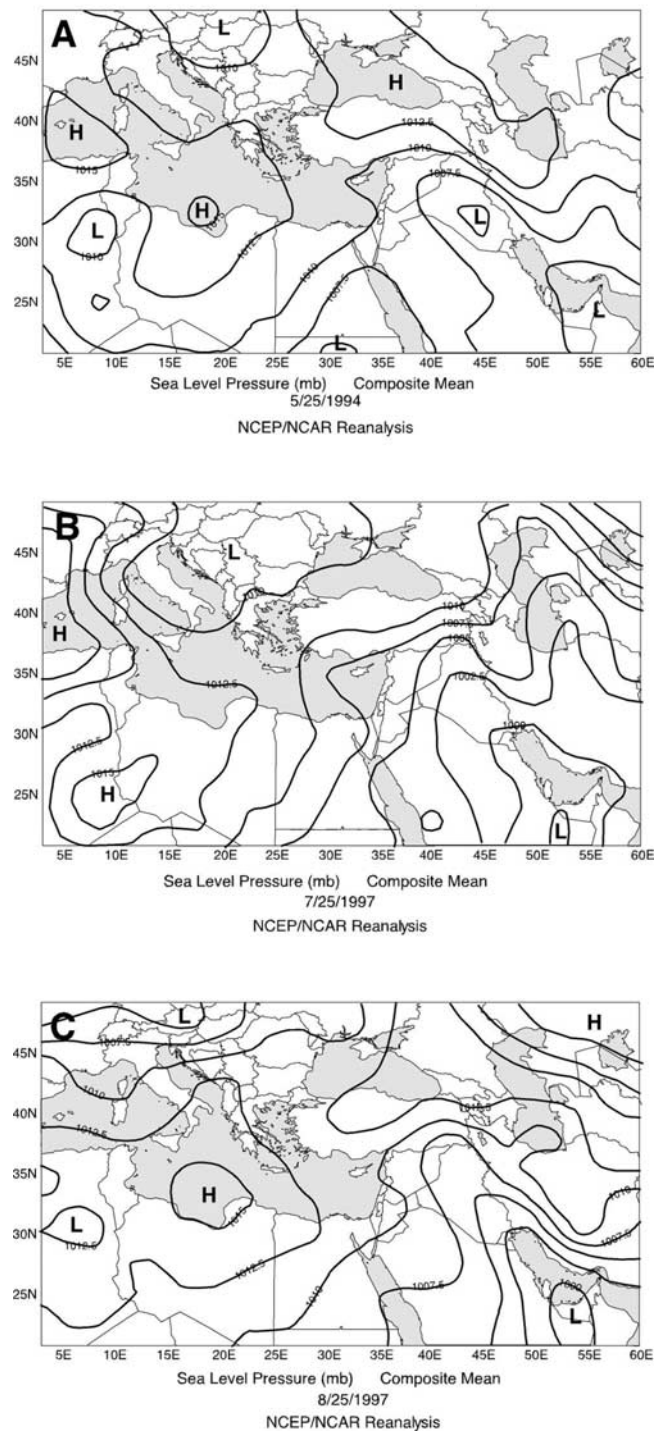


**Figure 8.** Synoptic maps of the three examined days (a) 25 May 1994, 1500 LST; (b) 25 July 1997, 1500 LST; (c) 28 August 1997, 1600 LST.

from the Tel Aviv metropolitan area toward Jerusalem, while keeping its initial rounded contours (as seen in Figures 5e and 5f). These three cases indicate that in summer, when synoptic gradient winds are weak as manifested by low ventilation-rate values, central inland Israel is strongly affected by elevated ozone levels caused by urban pollution plumes originating along the Mediterranean coastline.

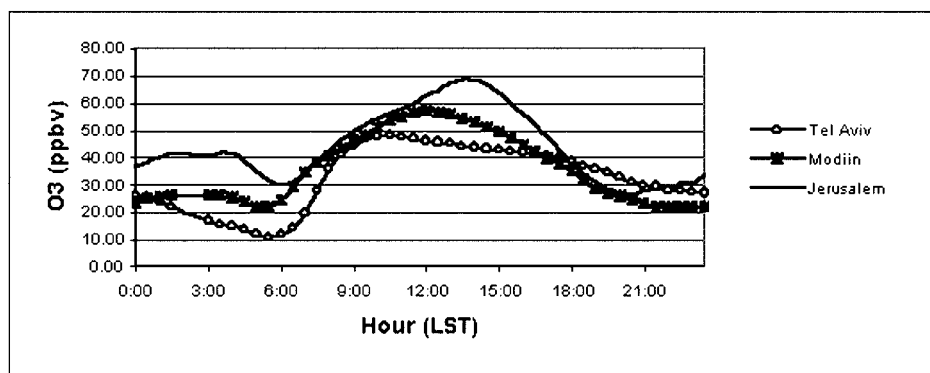


**Figure 9.** Averaged diurnal cycles of measured ozone concentrations in Tel Aviv, Modiin and Jerusalem for the periods of June–September in 1999 and 2000.

[38] Data for the other research flights, not reported in the study, further indicate that observational and model simulations were generally in phase, the degree of overlap dependent on the aforementioned arguments. Furthermore, during the summer period, elevated ozone concentrations were recorded over central Israel on almost all days studied. Both observations and calculations point to the Tel Aviv metropolitan region as the origin for the inland air pollution.

[39] Regarding the Gaza Strip transportation emission sources, the simulations suggested that the southern tail of the observed central Israel air pollution episodes are due to contributions from this region.

#### 5.4. Data Analysis of Ground-Based Monitoring Stations

[40] The available ground monitoring data were analyzed to discern any observable patterns for the pollution levels with increasing distance inland of the three monitoring sites. While data from the network were available only for two summer periods (June to September of 1999 and 2000), these periods were representative of the general situation existing during the summer month of the research period, since no significant changes have occurred since then in the area under investigation. Furthermore, considering time-space scales in ambient ozone and meteorology data [Estridge *et al.*, 1997; Rao *et al.*, 1997], the relevant long-term component (trend term) of the ozone time series, i.e., variations in climate, policy, and/or economics, is of no significance in our case. The monitoring data for the entire period under examination were averaged over 30-min time segments. Figures 9 and 2 show the data for ozone and  $\text{NO}_y$ , respectively. The ozone levels exhibited a distinct inland scale dependency. Ozone peaks at later hours (1130, 1300, and 1400 in Tel Aviv, Modiin and Jerusalem, respectively) and on average reaches higher levels (50 ppbv, 56 ppbv, 70 ppbv for Tel Aviv, Modiin, and Jerusalem, respectively) as progress is made inland. A comparison of the coastal  $\text{NO}_y$  spectra (Tel Aviv) to the inland  $\text{NO}_y$  profiles (Modiin and Jerusalem) discerns different dynamics for these locations. While the initial levels in the Tel Aviv metropolitan area are higher during the morning rush hour emissions, they experience a pronounced bleaching by the late morning sea breeze in comparison to inland locations, which level out at relatively higher midday concentrations. This may indicate,

in the absence of any alternative  $\text{NO}_y$  source, that the early morning  $\text{NO}_x$  produced by transportation sources in Tel Aviv is transported inland, providing additional  $\text{NO}_y$  to the regions in its path. These results correspond well with the dynamics of the inland-penetrating plume. The observed increase in ozone concentrations is attributed to ongoing photochemical transformations while traversing inland. Thus the superposition of the transported ozone cloud, originating from the coastal metropolitan traffic sources, with the native formed ozone results in the higher observed ozone levels.

#### 6. Conclusions

[41] Airborne measurements showed that central inland Israel is strongly affected by pollution originating along the Mediterranean coastline, where urban transportation sources play a pivotal role. The flight measurements, model simulations and ground-level monitoring all showed that under northwesterly winds, elevated ozone values can be found over central Israel. These findings establish a scenario in which the physical process of inland movement of pollutants in general, and ozone precursors in particular, is established. The Tel Aviv metropolitan area and possibly the Gaza Strip region emit transportation pollutants into the troposphere on a daily basis, initiating their subsequent photochemical transformation as they are transported downwind. Model simulations showed that about 60% of the detected inland ozone concentration is nourished by traffic emissions during the morning rush hours from the Tel Aviv metropolitan area.

[42] The assumption of a photochemically aged air mass regime may enable the application of multivariate linear regression analysis to quantitatively appraise ozone production over central Israel. Thus, under these conditions, the application of a relatively simple statistical analysis method for evaluating ozone concentrations may replace the need for comprehensive photochemical solvers.

[43] Air pollution, with ozone-generating processes, is among the most significant ecological impacts of modern age network transportation. The problem is especially acute in regions with poor dispersion conditions such as those existing in Israel during the highly photochemically active summer period. The work presented here demonstrates the

ability of interdisciplinary modeling systems to operate collectively as a prediction tool/tracing device, capable of successfully predicting air pollution hot spots. The model is now being expanded to include photochemical transformations that will enable simulating ozone formation under additional conditions. This prediction and analysis tool is expected to assist in the shaping of present and future transportation infrastructure, where air pollution in general, and ozone problems in particular, are to be considered.

[44] **Acknowledgments.** This study was funded under the U.S. Middle East Regional Cooperation (MERC) Program (USAID Award PCE-G-00-99-00037-00), project title "Transboundary Air-Quality Effects from the Urbanization of Israel-Gaza Mediterranean Coast". We would like to acknowledge the assistance provided by the Israeli Ministry of the Environment (air quality monitoring national network) and the Israeli Meteorological Service for providing the relevant air quality and meteorological data. We would also like to thank Robert Bornstein for helpful discussions and encouragement during the performance of the above research.

## References

- Dabdub, D., L. L. DeHaan, and J. H. Seinfeld, Analysis of ozone in the San Joaquin Valley of California, *Atmos. Environ.*, **33**, 2501–2514, 1999.
- Dayan, U., and L. Koch, Ozone concentration profiles in the Los Angeles Basin—A possible similarity in the buildup mechanism of inland surface ozone in Israel, *J. Appl. Meteorol.*, **35**, 1085–1090, 1996.
- Dayan, U., and J. Rodnizki, The temporal behavior of the atmospheric boundary layer in Israel, *J. Appl. Meteorol.*, **38**, 830–836, 1999.
- Dayan, U., R. Shenhav, and M. Graber, The spatial and temporal behavior of the mixed layer in Israel, *J. Appl. Meteorol.*, **27**, 1382–1394, 1988.
- De Fre, R., P. Bruynserade, and J. G. Kretzschmar, Air pollution measurements in traffic tunnels, *Environ. Health Perspect.*, **102**, 31–37, 1994.
- Eskridge, R. E., J. Y. Ku, S. T. Rao, S. P. Porter, and I. Zurbenko, Separating different scales of motion in time series of meteorological variables, *Bull. Am. Meteorol. Soc.*, **78**, 1473–1483, 1997.
- Finlayson-Pitts, B. J., and J. N. Pitts, Tropospheric air pollution: Ozone, airborne toxics, polycyclic aromatics, hydrocarbons, and particles, *Science*, **276**, 1045–1052, 1997.
- Fraser, M. P., G. R. Cass, and R. T. Brend, Particulate organic compounds emitted from vehicle exhaust and in the urban atmosphere, *Atmos. Environ.*, **33**, 2715–2724, 1999.
- Hashmonay, R., A. Cohen, and U. Dayan, Lidar observation of the atmospheric boundary layer in Jerusalem, *J. Appl. Meteorol.*, **30**, 1228–1236, 1991.
- Her Majesty's Stationery Office (HMSO), Economic assessment of road schemes: Cost benefit analysis (COBA) manual, in *Design Manual for Roads and Bridges*, vol. 13, Dep. of Transp., ISBN 0115516697, Norwich, England, UK, 1996.
- Hurley, P., and W. Physick, A Lagrangian particle model of fumigation by breakdown of the nocturnal inversion, *Atmos. Environ.*, **25A**, 1313–1325, 1991.
- INRO Consultants Inc., *Emme/2 User's Manual*, Software release 9, Montreal, Canada, 1998.
- Kleindienst, T. E., D. F. Smith, E. E. Hudgens, and R. F. Snow, The photooxidation of automobile emission: Measurements of the transformation products and their mutagenic activity, *Atmos. Environ.*, **26A**, 3039–3053, 1992.
- Kley, D., Tropospheric chemistry and transport, *Science*, **276**, 1043–1045, 1997.
- Koch, J., and U. Dayan, A synoptic analysis of the meteorological conditions affecting dispersion of pollutants emitted from tall stacks in the coastal plain of Israel, *Atmos. Environ.*, **26A**, 2537–2543, 1992.
- Lu, R., and R. P. Turco, Ozone distribution over the Los Angeles Basin: Three-dimensional simulations with the SMOG model, *Atmos. Environ.*, **30**, 4155–4176, 1996.
- Moussiopoulos, N., and S. Papagrigoriou (Eds.), Athens 2004 air quality, in *Proceedings of the International Scientific Workshop on "Athens 2004 Air Quality"*, 183 pp., FiatLux Publ., Fremont, Calif., 1997.
- Olszyna, K. J., E. M. Bailey, R. Simonaitis, and J. F. Meagher, O<sub>3</sub> and NO<sub>y</sub> relationships at a rural site, *J. Geophys. Res.*, **99**, 14,557–14,563, 1994.
- Olszyna, K. J., M. Luria, and J. F. Meagher, The correlation of temperature and rural ozone levels in southeastern U.S.A., *Atmos. Environ.*, **31**, 3011–3022, 1997.
- Orlanski, I., A rational subdivision of scales for atmospheric processes, *Bull. Am. Meteorol. Soc.*, **56**, 527–530, 1975.
- Peleg, M., M. Luria, I. Setter, D. Perner, and P. Russel, Ozone levels in central Israel, *Isr. J. Chem.*, **34**, 375–386, 1994.
- Physick, W. L., and D. J. Abbs, Modeling of summertime flow and dispersion in the coastal terrain of Southeastern Australia, *Mon. Weather Rev.*, **119**, 1014–1030, 1991.
- Pielke, R. A., W. R. Cotton, C. J. Tremback, W. A. Lyons, L. D. Grasso, M. E. Nicholls, M. D. Moran, D. A. Wesley, T. J. Lee, and J. H. Copeland, A comprehensive meteorological modeling system, *Meteorol. Atmos. Phys.*, **49**, 69–91, 1992.
- Pierson, W. R., A. W. Gertler, N. F. Robinson, J. C. Sagebiel, B. Zielinska, G. A. Bishop, D. H. Stedman, R. B. Zweidinger, and W. D. Ray, Real-world automotive emissions, Summary of Studies in the Fort McHenry and Tuscarora Mountain Tunnels, *Atmos. Environ.*, **30**, 2233–2256, 1996.
- Pilinis, C., P. Kassomenos, and G. Kallos, Modeling of photochemical pollution in Athens, Greece, Application of the RAMS-CALGRID modelling system, *Atmos. Environ.*, **27B**, 353–370, 1993.
- Rao, S. T., I. G. Zurbenko, R. Neagu, P. S. Porter, J. Y. Ku, and R. Henry, Space and time scales in ambient ozone data, *Bull. Am. Meteorol. Soc.*, **78**, 2153–2166, 1997.
- Roorda-Knape, M. C., N. A. H. Janssen, J. J. De Hartog, P. H. N. Van Vliet, H. Harssema, and B. Brunekreef, Air pollution from traffic city districts near major motorways, *Atmos. Environ.*, **32**, 1921–1930, 1998.
- Seinfeld, J. H., Urban air pollution: State of the science, *Science*, **243**, 745–752, 1989.
- Seinfeld, J. H., and S. N. Pandis (Eds.), *Atmospheric Chemistry and Physics: Air Pollution to Climate*, 1326 pp., John Wiley, New York, 1998.
- Silibello, C., G. Calori, G. Brusasca, G. Catenacci, and G. Finzi, Application of photochemical grid model to Milan metropolitan area, *Atmos. Environ.*, **25**, 2025–2038, 1998.
- Staehelin, J., C. Keller, W. Stahel, K. Schlapfer, and S. Wunderli, Emission factors from road traffic from tunnel measurements (Gubrist Tunnel, Switzerland), part III, Results of organic compounds, SO<sub>2</sub> and speciation of organic exhaust emission, *Atmos. Environ.*, **32**, 999–1009, 1998.
- Svensson, G., Model simulation of the quality in Athens, Greece, during the Medcaphot-trace campaign, *Atmos. Environ.*, **32**, 2239–2268, 1998.
- Trainer, M., et al., Correlation of ozone with NO<sub>y</sub> in photochemically aged air, *J. Geophys. Res.*, **98**, 2917–2925, 1993.
- Walko, R. L., C. J. Tremback, and R. F. A. Hertenstein, RAMS—Regional Atmospheric Modeling System version 3b, in *User's Guide*, ASTER Div., Mission Res. Coop., Fort Collins, Colo., 1995.
- U. Dayan and J. Kaplan, Department of Geography, Hebrew University of Jerusalem, Jerusalem 91905, Israel.
- A. W. Gertler, Desert Research Institute, P.O. Box 60220, Reno, NV 89506, USA.
- G. Kallos and P. Katsafados, University of Athens, Laboratory of Meteorology, Ippocratous 33, Athens 106 80, Greece.
- M. Luria, V. Matveev, and M. Peleg, Environmental Science Division, School of Applied Sciences and Technology, Hebrew University of Jerusalem, Jerusalem 91904, Israel.
- Y. Mahrer and D. O. Ranmar, Department of Soil and Water Sciences, Faculty of Agricultural, Food and Environmental Quality Sciences, Hebrew University of Jerusalem, Rehovot 76100, Israel.